Iron wool as a heating agent for magnetic catalysis: Experiments and analysis of heating properties under a high-frequency magnetic field

Salim Daccache, Sourav Ghosh, F. Marias, B. Chaudret, J. Carrey

Iron wool as a heating agent for magnetic catalysis: experiments and analysis of heating properties under a high-frequency magnetic field

S. Daccache[1], S. Ghosh[1], F. Marias[2], B. Chaudret[1] and J. Carrey[1,*]

[1] Laboratoire de Physique et Chimie des Nano-Objets (LPCNO), Université de Toulouse, INSA, CNRS UMR 5215, UPS, 135 av. de Rangueil, 31077 Toulouse Cedex 4, France

[2] Laboratoire de Thermique, Energétique et Procédés (LaTEP), Université de Pau et des Pays de l'Adour, CNRS EA 1932, Avenue de l'Université, BP 576 - 64012 Pau Cedex, France

* Corresponding author. : email : julian.carrey@insa-toulouse.fr

Abstract:

Magnetically induced heterogeneous catalysis has been attracting attention due to its high energy efficiency and flexibility for dynamic reactor control. Iron wool is a commercial, low-cost and versatile heating agent, which has been used in several magnetic catalysis studies, but its heating properties have never been investigated. Here, the properties of three types of Fe wool were studied using optical and electronic microscopy, X-Ray diffraction and measurements of both heating power and high-frequency hysteresis loops. The effects of strand width, packing, and magnetic field amplitude and frequency were studied. A maximum specific absorption rate (SAR) around 700 W/g under a rms field of 47.4 mT at 93 kHz was measured for the larger width Fe-wool. High-frequency hysteresis loops were used to quantify the contribution of hysteresis losses and eddy currents to the total heating. Eddy currents contribute 65-90% to the global heating depending on the strand width. Coating the wool with SiO_2 and Ni has negative effects on the SAR, but none on hysteresis losses. It is interpreted as originating from the cut-off of inter-wire eddy currents due to the insulating (SiO_2, oxidized Ni) nature of the coating. Lastly, it was found that adding more Fe-wool in a given volume mostly decreases SAR. This effect could be due to the absorption and/or screening of the field by surface strands, but also to magnetic interactions. The results described in this work give insights into the magnetic heating of microscale magnetic materials and optimize their use for heterogeneous catalysis.

I. Introduction:

The industrial sector is one of the leading greenhouse gas producers, with a 29.4% share of emissions worldwide in 2020[1], heat generation for industrial usage being a huge contributing factor (around two-thirds of industrial energy demand)[2]. One possibility to reduce the associated emissions is to switch to electrical heating methods (induction heating, infra-red, microwave) instead of fossil fuel-based ones. Indeed, electrical heating offers better performance, lower power consumption and the possibility of relying on low-emission energy sources such as green renewable electricity[3]. In addition, developing processes well adapted to the intermittent nature of renewable energies would be an advantage for manufacturers since the cost of electricity in a network with a large share of intermittent sources would vary a lot, and could even become negative, some industries being paid to stop using electricity during periods of low electricity production[4,5]. For this purpose, induction heating is highly promising, because of its extremely fast temperature sweeping rate, making possible a rapid ON/OFF switching of a process. In particular, power-to-gas applications, which aim to store the excess of renewable electricity under a chemical state (hydrogen, methane) would strongly benefit from such possibilities[6,7].

Induction heating (IH) or magnetic heating is a mature electrical heating technology that relies on the generation of an alternating magnetic field by a coil or an electromagnet, which in turn generates heat after being absorbed by adequate magnetic materials. Heat is generated by two main physical phenomena: eddy currents and hysteresis losses. Eddy currents are induced at the surface of magnetic materials leading to Joule heating[8]. This phenomenon is thus related to skin effect and skin depth. Hysteresis losses result from the magnetic response of the material to the external alternating magnetic field. Hysteresis losses are the product of the hysteresis loop area times the magnetic field frequency[9].

IH is usually dominated by eddy currents in large conducting bulk materials (slabs of metals, containers, tubes…) and has been used as source of heat in a variety of industries (food and beverage, pharmaceuticals, metal, cosmetics…)[8] as well as in everyday home applications (induction stoves). On the other hand, hysteresis loops contribute to most of the heating in nano-scale ferromagnetic or superparamagnetic materials[10–12], which has been gaining attention in the past decades for applications in hyperthermia cancer treatment[13,14], heterogeneous catalysis[15–17], and others[18–20].

In catalysis applications, IH makes it possible to heat the catalyst bed selectively and directly inside the reactor rather than bringing it from the outside by conventional means using intermediate heat carriers (heating fluids, reactor walls…). Thus, IH transforms the reactor into a "cold wall" reactor for which heat is brought only in useful regions, which presents numerous advantages[16] such as an increased energy efficiency and a reduction of heat transfer limitations as well as security and stability concerns[6]. Indeed, high local temperatures can selectively be reached at the surface of the catalysts in short times, which gives the opportunity to rapidly activate/deactivate the system and to better control the reaction[6]. This promising coupling between IH and catalysis has been called "magnetic catalysis".

Presently, most research and innovation in magnetic catalysis has been focused on magnetic nanoparticles, which would serve as both the catalyst and heating agent to activate the reaction.

A variety of reactions have been studied such as methanation[21,22], steam and dry methane reforming[23,24], hydrodeoxygenation[25] and pyrolysis[26]. Nanoparticles (NPs) offer several advantages when used as heating agents: high catalyst activity, high specific surface areas, and in some cases large SAR values[22,27,28]. For instance, NPs with SAR over 1000 W/g have been developed in our group[29]. Nonetheless, NPs present high production costs as well as low stability if not protected, which leads to coalescence, deactivation, and a decrease in both catalysis and heating properties[30]. These limitations are a major obstacle to the use of NP-based IH in industrial processes.

To overcome these problems, several groups have focused on studying and optimizing the heating properties of nano- and microscale particles, as well as researching new low-cost heating agents. One approach would be to use bigger sized materials to benefit from eddy currents generation, as well as their enhanced mechanical stability. Gomez-Polo *et al.* studied the magnetic heating of $Fe_{73.5-x}Cr_xSi_{13.5}Cu_1B_9Nb_3$ amorphous and nanocrystalline wires (with an average diameter of 130 µm) and the influence of Fe and Cr content on their SAR and Curie temperature (T_c) [31]. It was found that the highest SAR value was associated to the highest *T*c. In addition, having a *T*c close to the target temperature of a process decreases the SAR while providing useful self-regulating features. Morales *et al.* studied the heating power of $Fe_{2.25}Co_{72.75}Si_{10}B_{15}$ microwires (MWs) and registered SAR values between 1000 and 2800 W/g (it should be noted that the operating frequency was extremely high with f = 625 kHz)[32]. They were able to show that eddy currents are responsible for most of the heating, and that the length as well as the number of MWs influence the heating performance of the material.

Alonso *et al*[33] focused their study on the magnetic heating of FeCo nanowires and on the effect of their geometry (lengths and diameters varied respectively between 2-40 µm and 100-300 nm) on the resulting SAR. They showed that an increase of the wire length from 2 to 10 µm leads to an increase in the SAR from 350 to 1500 W/g (with $\mu_0 H$ = 30 mT and f = 310 kHz); it then slowly increases up to 1510 W/g at the maximum length of 40 µm. In addition, an increase in the diameter of the wires from 100 to 300 nm leads to an increase in the SAR of around 20%. Finally, they were able to demonstrate that a parallel alignment of the MWs with the generated field has a positive effect on the SAR. Talaat *et al.*[34] studied the heating properties of $Fe_{71.7}Si_{11}B_{13.4}Nb_3Ni_{0.9}$ glass-coated microwires for magnetic hyperthermia applications. They showed that a single 5 mm long wire presents a SAR of 521 W/g (under $\mu_0 H$ = 70 mT and f = 310 kHz). In addition, they studied the effect of the inter-wire distance as well as of their orientation with respect to the field. Their results show that increasing the distance between the wires leads to a decrease in the resulting SAR, while having them aligned to the magnetic field leads to an increase of the generated heat. These works show that high heating powers are achievable in micron-size magnetic materials. Nonetheless, such materials still present complex manufacturing methods and high costs, similarly to NPs.

In the present work, iron wool (Fe wool), a new low-cost heating agent for IH catalysis applications is investigated. It has been used in several studies of magnetically induced heterogeneous catalysis conducted by our group[18,35–37]. This agent is commercially available at low cost, with good magnetic and electric properties (permeability, conductivity, and magnetic saturation) and good physical resistance. However, its SAR values, mechanism of heating as well as the influence of various parameters on its heating properties have never been reported

yet. The aim of this work is to thoroughly investigate these parameters and mechanisms to provide a detailed and in-depth study of iron wool heating properties. This information would open up pathways for the optimization of Fe wool usage in gas and liquid-phase magnetically-induced heterogeneous catalysis and would help with any scale-up efforts down the line. In particular, the combination of calorific measurements and high-frequency hysteresis loops made it possible to distinguish between heating due to hysteresis losses and to eddy currents. Moreover, for many catalysis applications, additional layers of insulating or metallic materials must be added to the raw iron wool; it will be shown here that their influence on heating properties is significant. Finally, it will be shown that geometrical factors (diameter, length, density, orientation…) have a strong influence on heating properties, the knowledge of which is important for the design and the filling of catalysis reactors.

II. Materials and Methods:

1. Origin of products

Iron (Fe) wool of different wire thicknesses (Paille de fer MOYENNE, Paille de fer FINE, and Paille de fer SURFINE) was purchased from Gerlon (Abbevile, France). The three different types will be named thereafter Fe wool-M, Fe wool-F and Fe wool-SF. Bis (1,5-cyclooctadiene)nickel(0) ($Ni(COD)_2$, 98%) was obtained from Strem. Tetraethyl orthosilicate (TEOS, 99%), isopropanol (99.8%), and aqueous ammonia (28−30% NH_3 basis) were purchased from Sigma-Aldrich. Mesitylene (99.0%) was obtained from VWR. Mesitylene was dried on an alumina-desiccant solvent purifier and stored in the glovebox.

2. Coating of Fe wool by SiO_2 and Ni

The Fe wool modification has been carried out following a published protocol[35]. Briefly, silica (SiO_2) coating of Fe wool (Fe wool-SF or Fe wool-F) was carried out by base-catalyzed hydrolysis (sol-gel method) of TEOS in isopropanol during 7 hours with continuous stirring. This process was carried out five times to thicken the coating. Finally, the silica-coated sample was annealed under argon flow at 400°C for 5 hours. The samples were named Fe wool-SF@SiO_2 and Fe wool-F@SiO_2. Nickel deposition was carried out following the literature report by Ghosh *et al.*[35]. In a nutshell, $Ni(COD)_2$ was decomposed in the presence of Fe wool or Fe wool@SiO_2 in mesitylene at 150°C for 90 min under stirring. The samples were named Fe wool-SF@SiO_2@Ni and Fe wool-F@SiO_2@Ni. The silica and nickel-deposited sample abbreviations are shown in Table 1.

Table 1:Abbreviation of the samples

Abbreviation	Synthetic modification (if any)
Fe wool-SF	Iron wool SUPER FINE (commercial)
Fe wool-F	Iron wool FINE (commercial)
Fe wool-M	Iron wool MEDIUM (commercial)
Fe wool-SF@SiO_2	SiO_2 coating of Fe wool-SF
Fe wool-F@SiO_2	SiO_2 coating of Fe wool-F
Fe wool-SF@Ni	Ni deposition over Fe wool-SF
Fe wool-SF@SiO_2@Ni	Ni deposition over Fe wool-SF@SiO_2

3. Structural characterization

Powder X-ray diffraction (XRD) patterns were recorded using a PANalytical EMPYREAN diffractometer with cobalt Kα source (λ = 1.79 Å). The metal content of the samples was determined via inductively coupled plasma-atomic emission spectroscopy (ICP-AES) using an iCAP 6300 ICP Duo Spectrometer. Scanning electron microscopy (SEM) imaging was performed using a JEOL JSM-7800F microscope equipped with a field emission gun source. The energy-dispersive X-ray spectroscopy (EDS) elemental mappings were performed using a Bruker XFlash EDS detector attached to the SEM.

4. Colorimetric SAR measurements

Two devices were used to generate magnetic fields. The first (which will be referred to as equipment A from now on) is a commercial 93 kHz coil (Fives Celes, Lautenbach) with a maximum magnetic field intensity of 47.4 mT (rms value). The second, which will be referred to as equipment B, is a home-made coil set-up devoted to high-frequency hysteresis loop measurements[10]. It has also been used in this study to measure calorific SAR and compare the results with high-frequency hysteresis loop measurements. Equipment B can run on frequencies between 10 and 60 kHz, with field amplitudes up to 55 mT (0-peak value).

Calorimetric SAR measurements were obtained using the following protocol. The samples were loaded into glass tubes of 0.3 cm in diameter. Considering the high porosity and anisotropic nature of iron wool, special attention was paid to the loading method to get approximately the same volume of samples in each measurement. To this end, the iron wool was weighted, morphed into a cylindrical shape and introduced into the tube. Once in the tube, the sample was then carefully compressed until it reached a height of 1 cm and an approximate diameter of 0.3 cm. 1 mL of water was then added into the tube.

The tube is then introduced inside a sample holder made of insulating materials, to limit the heat losses towards the atmosphere. A fiber optic temperature probe (Reflex 4, Neoptix) is introduced inside the tube and carefully located at the midway point between the top of the iron wool sample and the water surface. SAR measurements are then conducted by turning on the magnetic field at the desired value for a set time interval (Δt) while measuring the temperature rise of the water (ΔT) using the temperature probe. Since water was used as the heat transfer media, we limited the maximum temperature to 60^0C to avoid any boiling (some boiling occurs at the surface of the iron wool when the average temperature exceeds 60°C). The SAR is then calculated using the following equation:

$$SAR\ (W/g) = \frac{C_{p,water} * m_{water}}{m_{iron\ wool}} * \frac{\Delta T}{\Delta t} \quad (1)$$

where $C_{p,water}$ is the heat capacity of water, m_{water} the weight of water added to the tube, $m_{iron\ wool}$ the weight of iron wool in the tube, ΔT the increase in water temperature and Δt the time of magnetic field application.

5. High-frequency hysteresis loop measurements

High-frequency hysteresis loop measurements were conducted on the different Fe wool samples using equipment B. The same loading methodology was used for the sample preparation. The measurement protocol has been described by Connord *et al.*[10].

III. Results

In the frame of the study, special attention was paid to the factors that govern the magnetic heating of Fe wool. Since such material might be used in packed beds and under varying field conditions, we decided to study both geometrical factors such as strand length/ diameter, density of the packed bed or alignment with the external field as well as factors like the frequency/amplitude of the applied magnetic field and the effect of adding surface layers on the Fe wool. In this section, the major results are described.

1. Preliminary considerations on the heating power amplitude

Before turning to experimental results, theoretical estimates of the eddy currents heating in iron microwires are provided. Our aim here is to show briefly why it is expected to find experimentally a contribution of eddy currents to the total heating. A simplified calculation of eddy currents for one isolated Fe wool-SF strand as well as simulations using the software FEMM are presented. Basic theoretical aspects concerning the link between the hysteresis losses and high-frequency hysteresis loop measurements will also be mentioned.

In the case of eddy current heating, heat generation is due to the induced electrical currents at the surface of the ferromagnetic material. A simplified equation for the eddy current heat generation is given by[38]:

$$P_{eddy} = \frac{\pi^2 B^2 d^2 f^2}{6k\varphi\rho} \quad (2)$$

where P_{eddy} is the generated heat in W/kg, B is the peak magnetic field density inside the sample in T, d is the sample diameter in m, f the field frequency in Hz, k is a shape factor equal to 2 in the case of an isolated wire, φ the resistivity in Ω.m and ρ the density of the sample in kg.m^{-3}.

Equation 2 is valid for a complete penetration of the magnetic field inside the material. In other words, skin effect is neglected. It means that this equation provides an upper value for the heating power and can lead to very large discrepancies at high frequencies and in bulk ferromagnetic materials. This equation provides a value for the SAR of around 400 W/g for a 100 µm in diameter wire under a field of 47.4 mT at 100 kHz.

Micromagnetic simulations were also conducted using the FEMM software. FEMM is a free-to-use suite of programs that solves static low-frequency electromagnetic problems on two-dimensional planar and axisymmetric domains using Maxwell's equations and the method of finite elements. The calculated SAR due to eddy currents is around 170 W/g under the same conditions. The details of the simulations as well as the parameters used for the equation can be found in Supplementary Materials section 3.

The results of both Equation 2 and FEMM simulations indicate that eddy currents can contribute to the magnetic heating of Fe-wool strands.

In the case of hysteresis loop heating, one might estimate the heat generation according to equation[9]:

$$P_{cycle} = Af \quad (3)$$

where P_{cycle} is the heat generated by hysteresis losses in W/kg, f the frequency of the applied field in Hz, and A the area of the hysteresis loop in J/kg. The hysteresis loop area cannot exceed 4 $\mu_0 H_{app}$ σ_s, where $\mu_0 H_{app}$ is the applied magnetic field in T and σ_s the saturation magnetization in Am^2/kg. The maximum value of hysteresis losses cannot therefore exceed 4132 W/g for an iron nanowire under the same conditions as above. In practice, experimental values of heating are often much lower than the theoretical maxima[9].

2. Structural and magnetic characterizations

a. Optical microscopy

Three different commercial types of Fe wool were used in our studies. Optical microscope images were analyzed to measure the average width of each Fe wool type as well as the homogeneity of the products. The image processing software ImageJ was used to determine the average strand width. For each Fe wool type, 15 optical microscope images were processed with ImageJ, and 4 to 6 strands were measured by image. Figure 1 shows typical images of the samples. Figure 2 presents the distribution of strand width for each type of Fe wool.

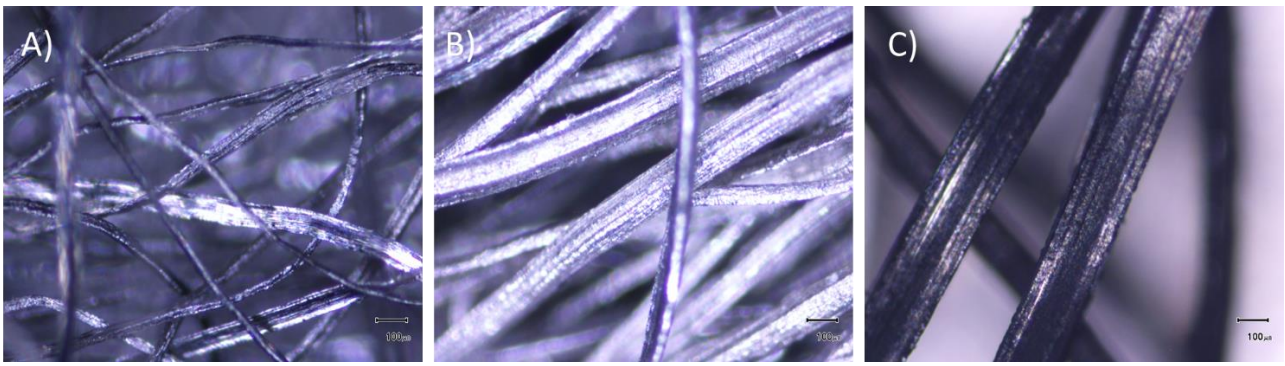

Figure 1: Optical microscope images of Fe wool A) SF, B) F and C) M samples. Scale bars on the images represent 100 µm.

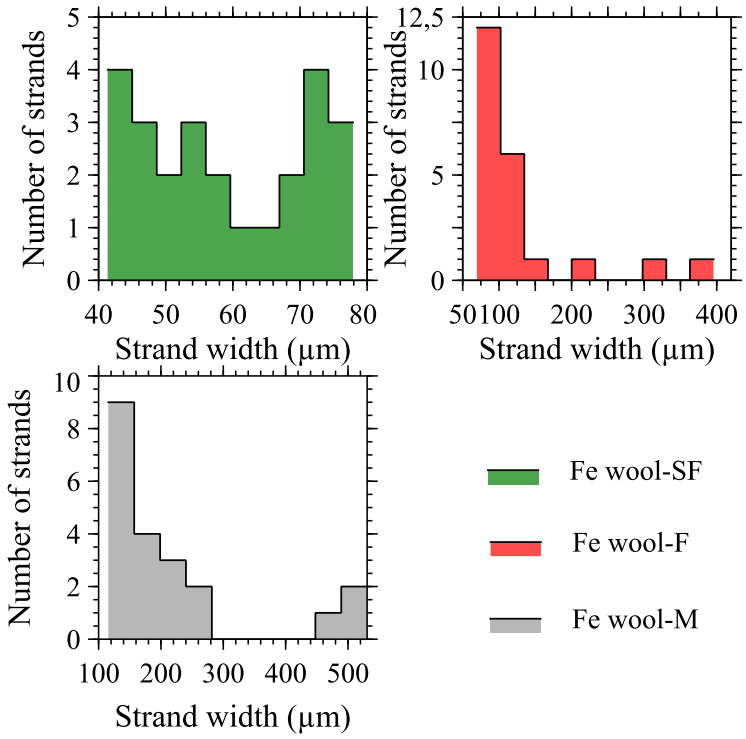

Figure 2: Strand width distribution for the three types of Fe wool.

Figure 2 shows that the Fe wool-SF samples present the highest homogeneity, with strand widths between 40 and 80 µm and a somewhat even distribution. In contrast, the F and M Fe wool samples show a lower homogeneity. In the case of the Fe wool-F samples, the widths range from 60 µm to 400 µm, the highest density lying between 60 and 150 µm. For the Fe wool-M, the widths range from 100 to 550 µm, the highest density lying between 100 and 250 µm. The calculated average width is around 60 µm for the SF samples, 125 µm for the F samples and 225 µm for the M samples.

To improve the reproducibility of our various measurements, these observations were taken into consideration while preparing the F and M samples. Special care was taken to withdraw the extremely wide strands in the case of the F type (strands between 300 and 400 µm) and the M type Fe wool (strands larger than 450 µm). They were manually removed from the samples before the measurements.

b. Structural properties and chemical analysis

The commercial Fe wool was functionalized with Ni and SiO_2 layers following Gosh *et al.* protocol[35]. The XRD patterns of the commercial and functionalized powdered Fe wool are shown in Figure S1 of S.M. All the diffraction patterns match well with the bulk body-centered cubic phase of bulk iron (ICDD: ICDD: 00-006-0696). Additional diffraction peaks corresponding to nickel were not observed, as previously reported by our team on similar samples[35]. The Fe content of commercial Fe wool was measured to be >99.8%, while the nickel deposition over Fe wool-SF and Fe wool-SF@SiO_2 are ~2wt% and ~3wt%, respectively[35] (see the ICP elemental analysis results in S.M. Section 1 Table S1).

The SEM images, EDX spectrum, and SEM-EDS elemental mapping of raw and functionalized Fe wool are shown in S.M. Figs. S2-S8. Si and Ni are detected in the SiO_2- and Ni-deposited samples (see SEM images, EDX spectrum, and SEM-EDS elemental mapping in S.M. Section 1 Figs. S5-S8). The EDS elemental mapping shows an even distribution of the SiO_2 layers in Fe wool-SF@SiO_2 and Fe wool-F@SiO_2 (see S.M. Section 1 Figs. S5-6). In the case of Fe wool-SF@Ni nickel dispersion is irregular, whereas Ni is evenly distributed in Fe wool-SF@SiO_2@Ni (see Figure 3 and S.M. Section 1 Fig. S7)[35].

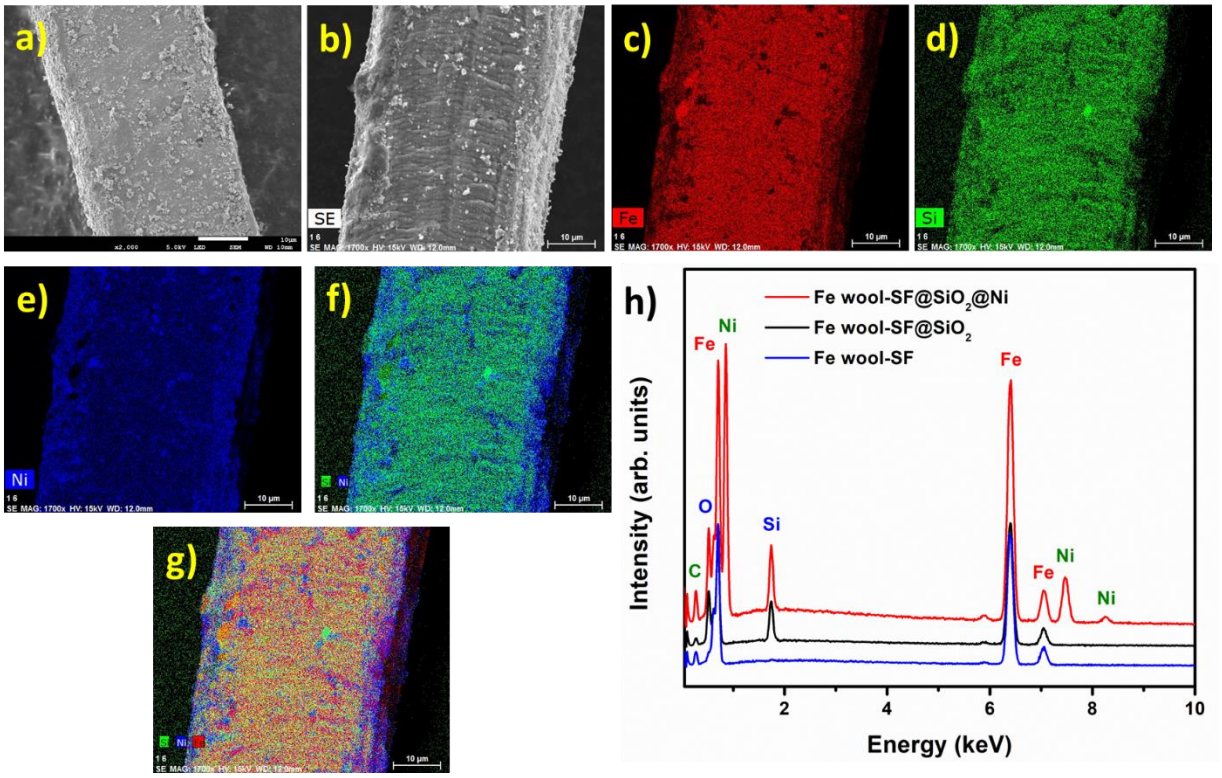

Figure 3: a) SEM image of the Fe wool-SF@SiO_2@Ni, b-g) SEM image and EDX elemental mapping of the Fe wool-SF@SiO_2@Ni. b) is the secondary electron image and c-g) the mapping, with Fe in red, Si in green, and Ni in blue. h) EDX spectral stack plot of the Fe wool-SF@SiO_2 before and after nickel and silica deposition.

c. Static magnetic properties

Vibrating sample magnetometry (VSM) measurements were conducted on the different Fe wool types (M, F and SF). Measurements up to 5 T have been published by our group and show that the saturation magnetization Fe-wool-SF equals 210 $Am^2.kg^{-1}$, as expected for a pure iron object[35]. Measurement results on the three types of wool at a lower magnetic field of 0.15 T are reported in Figure 4.

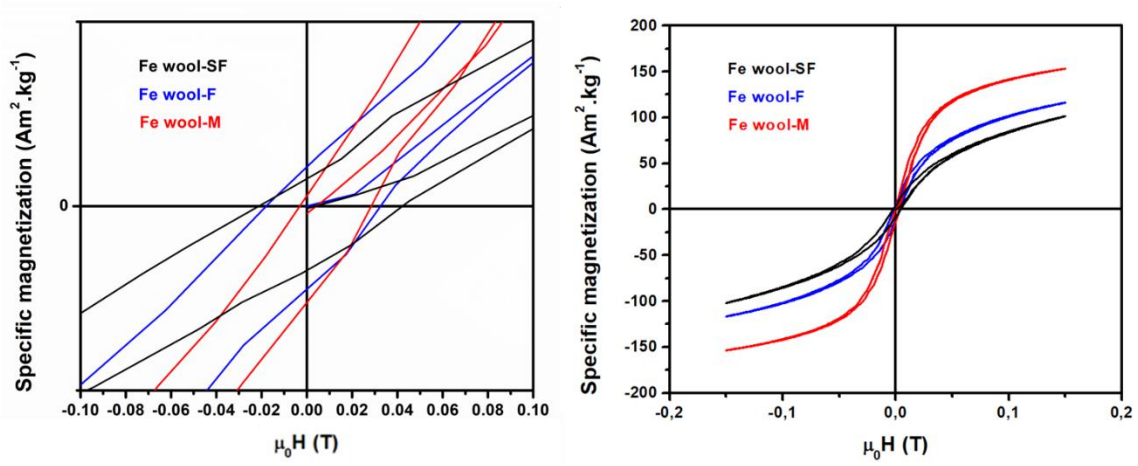

Figure 4: (a) and (b) VSM measurements for the three different Fe wool sizes. (a) Enlarged view of (b) at low fields.

These measurements show that strand thickness has no clear effect on the coercive field of the sample, the three types of samples displaying values around 0.03 T (more precise measurements under lower field amplitudes at high-frequency will be presented later in this work). On the other hand, the strand thickness exhibits significant influence on the magnetic susceptibility of the samples, the latter being larger for wider strands. Quantitatively, the slope at the origin is approximately two times larger for the M sample than for the SF one. This difference in magnetic susceptibility is attributed to the decrease in anisotropy of the samples with the increase in strand width: the individual Fe thin wires having a higher shape anisotropy than the larger ones, this would cause a globally larger saturation field in the Fe wool-SF since it is composed of an assembly of high anisotropy wires.

1. Effect of sample geometry on the measured SAR

Our group has an important background on the evaluation of the heating properties of magnetic nanoparticles for biological and catalysis applications and has developed adequate protocols for this purpose[39]. However, measuring the heating power of iron wool brings some additional complexity compared to nanoparticles, because of the influence of two geometrical factors: the strand orientation and the aspect ratio of the sample. Their influence must be well understood to perform reproducible and interpretable measurements. This is precisely the aim of the following paragraphs.

a. Effect of Fe wool strand orientation

The orientation of the Fe wool strands with respect to the generated magnetic field is a parameter that can be controlled while packing the sample. To study its effect on the heating, a single long strand of Fe wool-M (around 10 cm in length) was weighed (23 mg) and packed once in a vertical configuration and then in a horizontal one inside the coil. For both packing configurations, a diameter of 0.3 cm and a height of 1 cm was preserved. The packing configurations can be seen in S.M. Section 9 Fig. S15. SAR measurements were conducted using equipment A on both the F and M Fe wool samples. Figure 5 shows the SAR amplitude as a function of magnetic field in both configurations for the M sample.

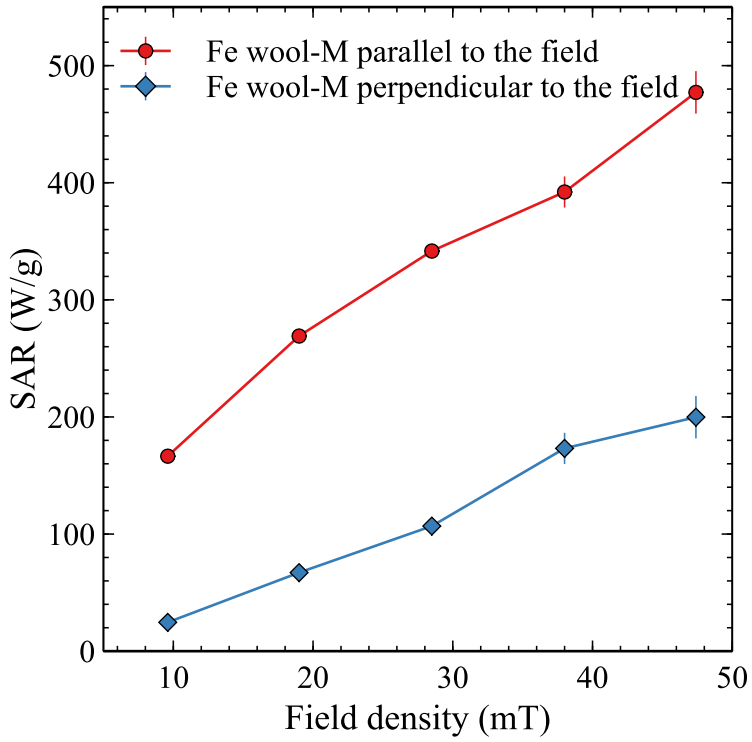

Figure 5: Calorific SAR measurement using equipment A on 23 mg of Fe wool-M. The configurations where the strand is parallel or perpendicular to the applied magnetic field are compared.

The results for the Fe wool-M sample show a clear effect of the strand configuration on the measured SAR. When Fe wool strands are parallel to the external applied field a larger heat release is observed compared to the horizontal configuration. For example, under a 9.6 mT field, SAR values of 166 W/g and 25 W/g were measured for the vertical and horizontal configurations respectively (which represents an 85% decrease). Under a 47.4 mT field, SAR values of 477 W/g and 199 W/g were measured (59% decrease). Qualitatively similar results were observed for the Fe wool-F sample (see S.M. Section 4 Fig. S.10). These results are in accordance with the findings from other researchers that demonstrates the effect on SAR of aligning nano- or micro-wires with magnetic field[33,34]. This effect likely originates from shape anisotropy, the susceptibility of the samples being larger when the strand is aligned with the external magnetic field. Given these considerations, parallel packing of the Fe wool strands was used in what follows.

b. Effect of Fe wool strand length

The medium Fe wool was used to study the effect of strand length on SAR. A long strand of Fe wool with a mass m = 21 mg and a length l = 8.5 cm was chosen for the measurements. At first, the strand was cut into 8 equal pieces, then 16 and finally into 32 small strands and SAR measured in each configuration. Figure 6 shows SAR measurements using equipment A, for field values ranging between 9 and 47 mT for the different strand lengths.

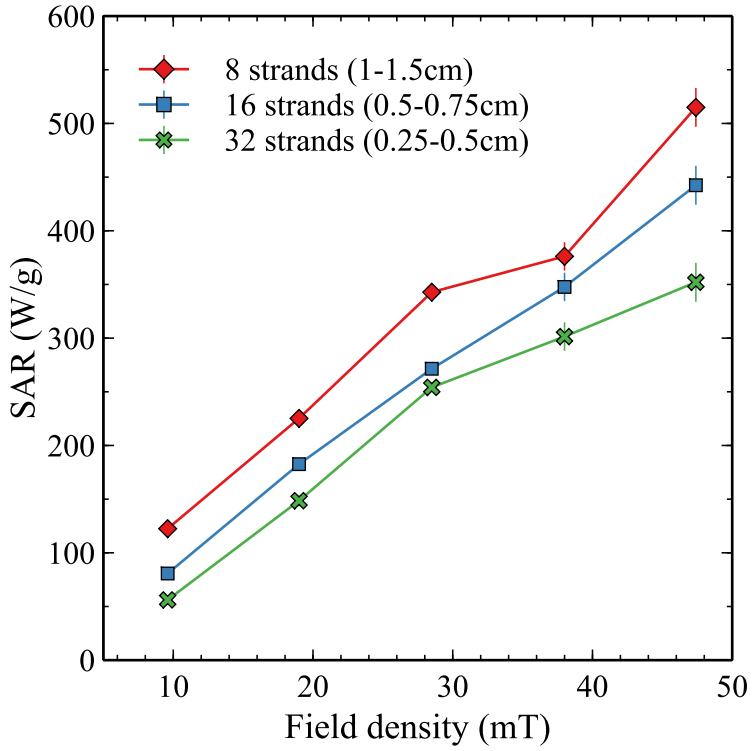

Figure 6: SAR measurements on sample M as a function of magnetic field for different strand lengths. Measurements were performed on equipment A. *m* = 21 mg.

A clear effect of strand length on heating power is observed. When the 8 strands (of lengths between 1 and 1.5 cm) were cut into 16 smaller ones (of lengths between 0.5 and 0.75 cm), the SAR decreased from 530 W/g to around 440 W/g. Further division of the sample into 32 strands (lengths ranging between 0.25 and 0.5 cm) led to a SAR decrease down to 350 W/g. Once again, the decrease in heating power with the length of the sample can be attributed to the link between the strand length and its magnetic susceptibility (i.e. shape anisotropy). Alonso et al.[33] showed that increasing the length of nanowires leads to an increase in their susceptibility, in line with our findings.

2. Effect of Fe wool strand thickness on the heating power and mechanisms

In this section the effect of the Fe wool strand thickness on the heating power amplitude is studied. In addition, high-frequency hysteresis loop measurements are used to shed some light on the respective contribution of hysteresis losses and eddy currents to the total heating.

1. Influence of Fe wool strand thickness on total heating power

To study the effect of strand thickness on the heating of Fe wool, calorific SAR measurements using equipment A were performed using 15 mg samples under different magnetic field amplitudes. Figure 7 shows the resulting SAR for each type of sample for a magnetic field ranging between 9.6 and 47.4 mT.

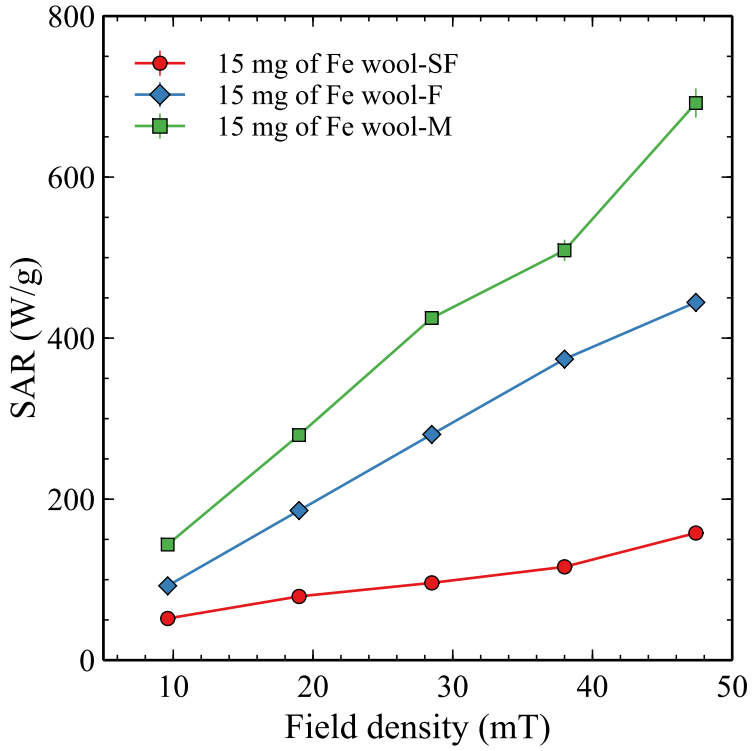

Figure 7: Calorific SAR measurement as a function of magnetic field for three different Fe wool widths. Measurements were performed on equipment A. m = 15 mg, f = 93 kHz.

It can be clearly observed that the SAR increases with the Fe wool strand thickness. For instance, at 47.4 mT, the SF, F, and M have SAR values of 160 W/g, 440 W/g and 700 W/g, respectively. The same measurements were conducted using equipment B for two different values of the applied frequency (16 and 50 kHz, see S.M. Section 5 Fig. S11). The same trend was observed.

This increase could be explained by two different mechanisms. Firstly, static magnetic measurements displayed in Figure 4 show that the magnetic susceptibility increases with strand width, which should in principle increase both hysteresis losses and eddy currents. Secondly, Equation 2 shows that the wire diameter is also responsible for a direct increase of the eddy currents, independently of a susceptibility increase. This is due to the increase of surface area available for the creation and circulation of eddy currents, which in turn increases the heat generated by Joule effect. The experiments described below aim at separating these different contributions.

2. High-frequency hysteresis loop measurements

High-frequency hysteresis loop measurements are very important as they provide information on the magnetic response of magnetic objects like the ones used in magnetic catalysis and magnetic hyperthermia applications and to get access to the hysteresis losses amplitude only[10,17]. Typical measurements performed on the SF sample using equipment B are shown in Figure 8. Similar results to the ones described in Figure 8 were observed for the other Fe wool types and can be found in S.M. Section 6 Fig. S12.

Figure 8a) shows hysteresis loops observed under a 50 kHz frequency for magnetic field values ranging from 5 to 48 mT. Results are similar to the ones previously observed on magnetic nanoparticles and consist in minor loops imbricated one into another. Interestingly, hysteresis loops have a square shape with a saturation-like behavior, except that the magnetization value at which the curves seem to saturate (roughly 6 Am^2/kg) is much lower than the saturation magnetization of iron (220 Am^2/kg). This might be attributed to the fact that only minor parts of the sample are able to react and get reversed at such a high frequency and low magnetic field. The global magnetic response of the sample is therefore strongly reduced.

Figure 8b) displays the hysteresis loops observed for the Fe wool-SF sample under varying frequencies (16, 22, 39 and 50 kHz) at a constant magnetic field of 19 mT. As expected, a significant frequency dependence of the coercive field is observed: it increases from around 6 mT under 16 kHz to around 11 mT under 50 kHz. On one other hand, no major variation of the sample average magnetic susceptibility (linked to magnetization value at the maximum applied magnetic field) was detected as a function of the applied frequency.

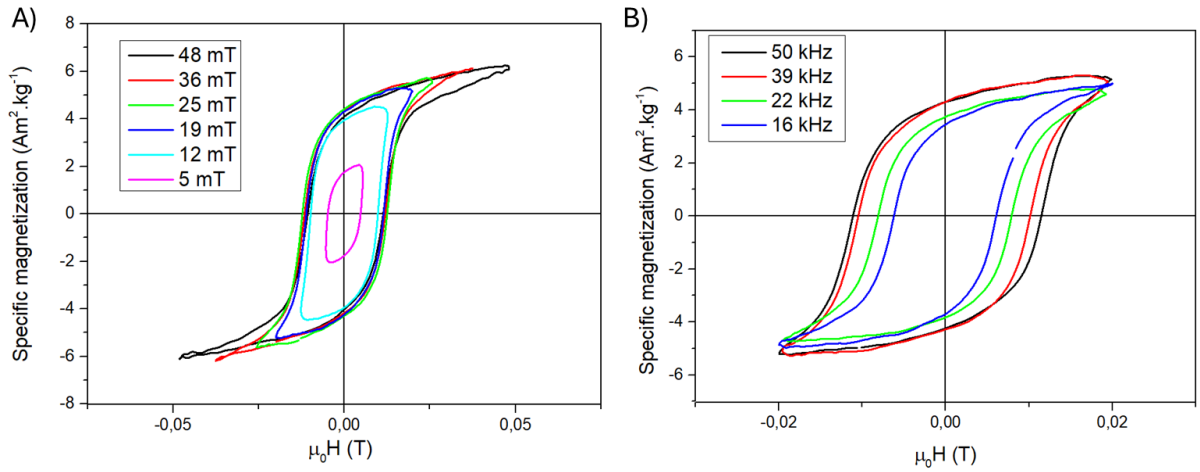

Figure 8: High-frequency hysteresis loops of Fe wool-SF as a function of A) magnetic field amplitude under a 50 kHz field frequency, and B) as a function of frequency under a 19 mT field density. Measurements were performed using equipment B.

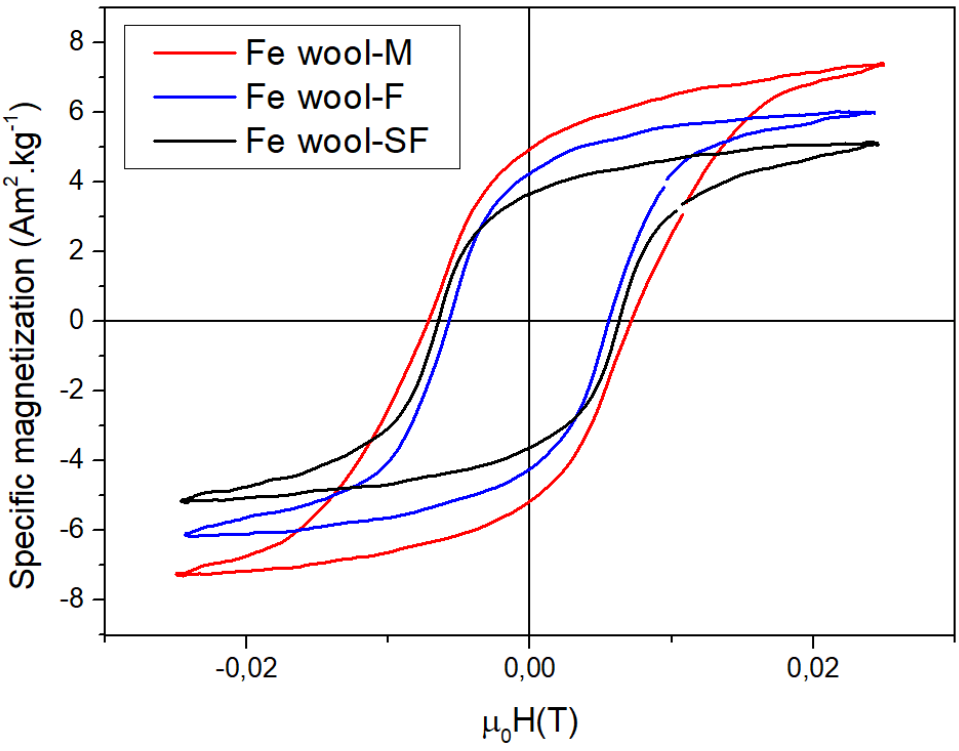

Figure 9: High-frequency hysteresis loop measurements for the three different Fe wool sizes. Measurements were performed on equipment B under a field of 16 kHz and 25 mT.

Figure 9 shows the hysteresis loops measured under a field of 25 mT and a frequency of 16 kHz for the three Fe wool samples. No clear and reproducible influence of the strand thickness on the coercive field could be assessed from our measurements among the various samples. However, an increase of the average susceptibility with strand thickness - as in Figure 9 - was systematically observed. This finding is in accordance with the static VSM measurements previously shown in Figure 4.

3. Eddy current vs hysteresis loop heating contribution

As already discussed in the introduction, magnetic heating is caused by eddy currents and hysteresis losses. The latter can be deduced from the integration of the high-frequency hysteresis loop measurements performed on equipment B. In addition, the latter allows us to measure the calorimetric SAR under the same conditions. The contribution of eddy currents to the total sample heating can therefore be estimated. Figure 10 presents the results of such an analysis. The provided values are the average of the contributions for different field amplitudes. To validate our measurement setup and analysis, we also measured a control sample consisting in a standard colloidal solution of nickel/cobalt nanoparticles synthesized in our laboratory. In such a sample, the eddy current contribution is expected to be null. For this sample, both the cycle heating and the calorific SAR were around 10 W/g, confirming the validity of our approach (see Figure 10). The high-frequency loop of this control sample is shown in S.M. Section 7 Fig. S13.

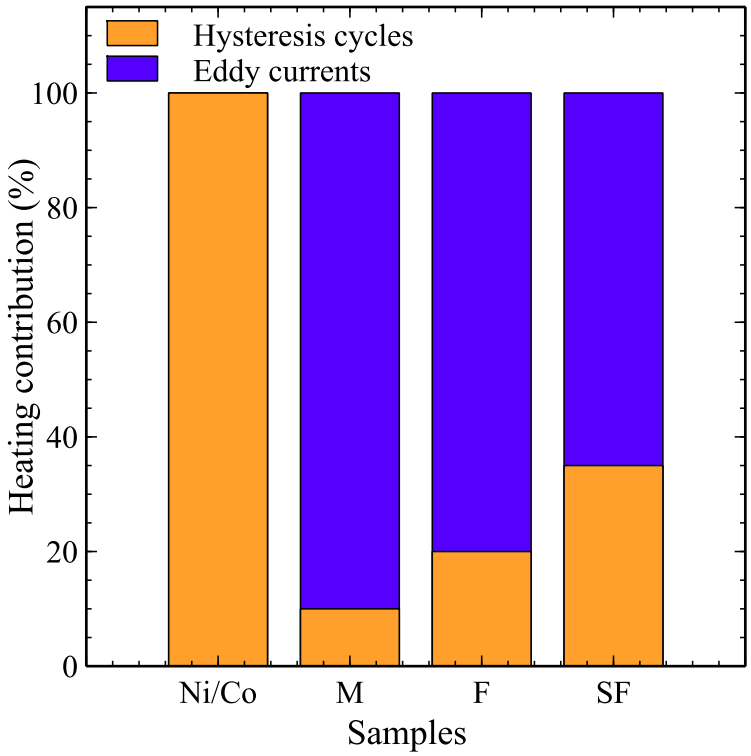

Figure 10: Eddy current and hysteresis loop contribution (averaged under different magnetic field amplitudes ranging between 5 and 48 mT) to the heating for different types of Fe wool under a 50 kHz field.

Figure 10 evidences a clear difference between the various samples. The M sample has the highest eddy current contribution (90%), followed by the F sample (80%) and then the SF one (65%). The same types of results were observed at other frequencies, with a slight increase in the eddy current contribution with the increase in frequency for all Fe wool samples (for example going from 85 to 90% with an increase of frequency from 16 to 50 kHz for the Fe wool-M sample).

4. Effect of Fe wool functionalization on the heating power and associated mechanisms

In some heterogeneous reactions, adding surface layers on the Fe wool strands could be beneficial by inferring catalytic activity to the heating agent[35]. The effect of adding two different types of surface layers was studied. Silica (SiO_2) and nickel (Ni) were deposited on the surface of SF and F Fe wools, and the calorific SAR as well as hysteresis loops were measured.

In the case of Fe wool-SF, the SAR of 20 mg of four different samples was measured : regular Fe wool-SF; Fe wool-SF with a silica coating (Fe wool-SF@SiO_2); Fe wool-SF with a nickel coating (Fe wool-SF@Ni) and finally Fe wool-SF with both nickel and silica coatings (Fe wool-SF@SiO_2@Ni). Figure 11 shows the SAR values measured for the four different samples of Fe wool-SF as a function of magnetic field amplitude.

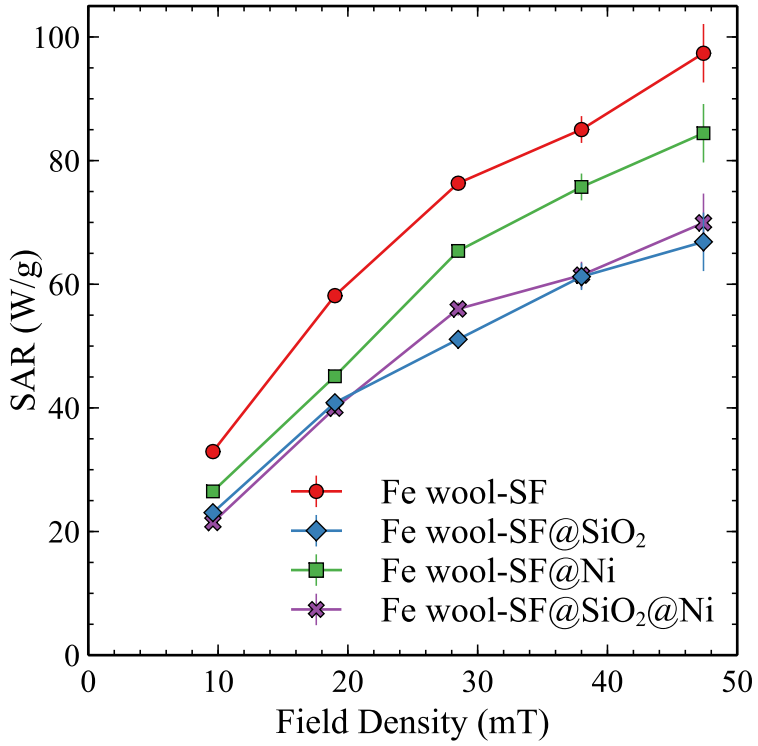

Figure 11: SAR as a function of field amplitude for Fe wool-SF samples with different surface coatings. m = 20 mg, f = 94 kHz. Measurements were performed using equipment A.

These results clearly show that the addition of coatings on the Fe wool influences its heating power. The Fe wool-SF sample with no added surface layers presents the highest SAR values with 158 W/g at 47.4 mT. Adding a nickel coating decreases this value to around 108 W/g, while adding a silica one further decreases it to around 84 W/g. Furthermore, adding both a silica and nickel layer has the same effect as adding a simple silica one and decreases the SAR to around 82 W/g.

The effect of adding a silica layer was also studied in the case of 20 mg sample of Fe wool-F. Figure 12 shows the SAR as a function of magnetic field for the regular and the silica-coated Fe wool-F. The samples have a similar trend to that observed in the case of the Fe wool-SF. Under a 47.4 mT field, the measured SAR decreases from 444 W/g for Fe wool-F to 334 W/g in the case of the Fe wool-F@SiO_2.

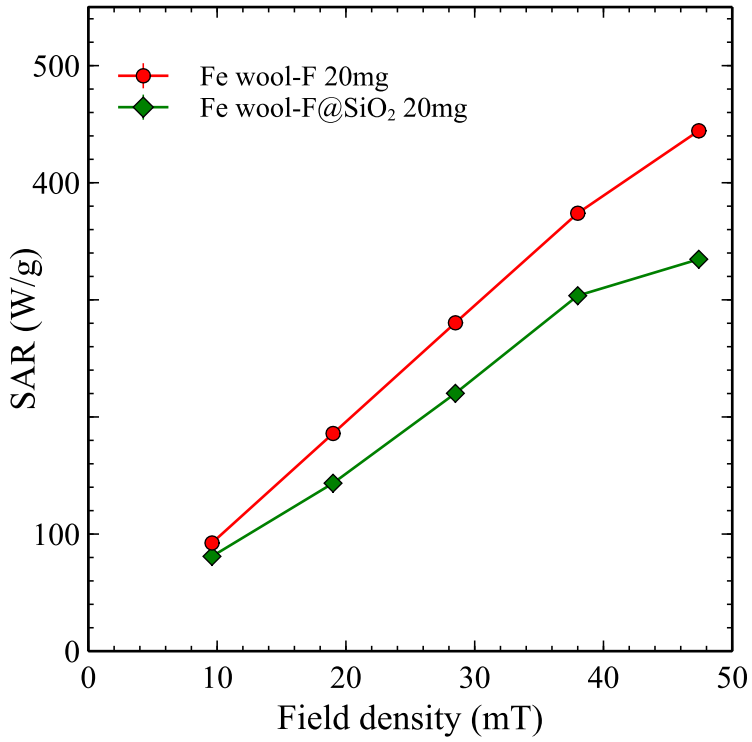

Figure 12: SAR as a function of magnetic field for 20 mg samples of regular and silica-coated Fe wool-F. Measurements were performed using equipment A at 94 kHz.

To get a better understanding of this effect, we conducted both high-frequency hysteresis loop measurements and calorimetric SAR measurements using equipment B for the Fe wool-F and Fe wool-F@SiO_2 samples.

Measurements were carried out using equipment B under four different field frequencies (16, 22, 39 and 50 kHz) with a field ranging from 5 to 48 mT. The measured cycles were then used to estimate the hysteresis losses contribution to the overall heating (see Figure 13). The calorimetric SAR in Figure 13 is in accordance with the measurements presented in Figure 12 using equipment A. The Fe wool-F sample has the higher SAR values (75 W/g at 49 mT), while the Fe wool-F@SiO_2 sample has a SAR of around 50 W/g. Conversely, the hysteresis losses are nearly identical for the two samples with a value of around 9.5 W/g under a 49 mT field. Similar results were also observed for other field frequencies.

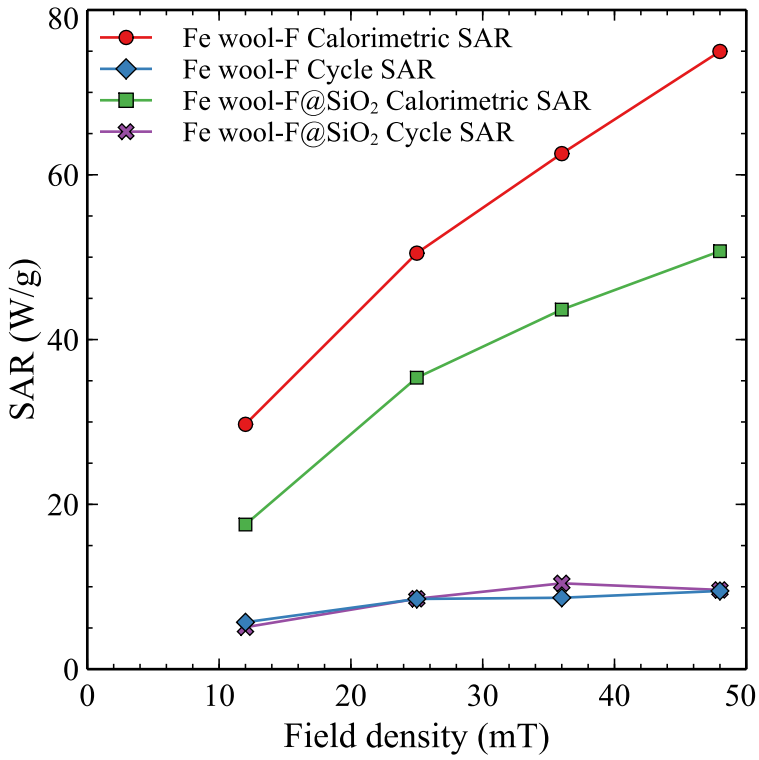

Figure 13: Comparison between calorimetric SAR and hysteresis losses for the Fe wool-F and Fe wool-F@SiO_2 samples. Measurements were performed on equipment B at 39 kHz.

We interpret these results as originating from the insulating nature of the SiO_2 surface layer, which would strongly reduce eddy currents. Since the intra-wire eddy currents are not expected to be significantly modified by adding a surface layer, our hypothesis is that the inter-wire eddy currents would be cut off by the insulating layer. Conversely, the measured hysteresis loops were identical for both Fe wool samples. This is coherent with the fact that a thin SiO_2 layer deposited on a micron wide wire is not expected to influence significantly its magnetic properties.

As illustrated in Figure 11, adding a Ni layer to the samples has also a detrimental effect on heating power, although less important than in the case of SiO_2. Here again, since nickel spontaneously oxidized into an insulating NiO layer under ambient atmosphere, we assume that this oxide layer cuts-off inter-wire eddy currents. The fact that the effect is lower than for SiO_2 could reasonably be explained by the incomplete coverage of the wires by Ni compared to SiO_2 (see S.M. Section 1 Figs. S5 and S7).

5. Influence of Fe wool weight on heating power

This last section is devoted to the discussion of a very important parameter for the catalysis application: the influence of the quantity of iron wool inside the coil. Indeed, in a catalysis experiment, the maximum temperature which can be reached is strongly influenced by the magnetic field frequency and amplitude as well as by the type of iron wool. The former is determined by technical or economical consideration. For the latter, our experimental results presented above indicate that the different sizes of Fe wool have relatively high SAR values even at low frequencies. To reach high temperatures, one would expect that it is sufficient to

increase the quantity of iron wool inside the reactor. One would indeed expect a simple linear relationship between the heat generated by the iron wool and its quantity. It will be shown in the present section that this is not the case and that rather complex considerations need to be taken into account.

Heating power measurements were conducted using equipment A with different amounts of SF Fe wool. During these experiments, special attention was paid to preserve the same total volume and shape of the samples to avoid any influence of shape on the results. Figure 14 shows the SAR as well as the total generated power of different mass of Fe wool-SF under a 9.6 mT and a 47.4 mT field. Similar measurements were conducted on the M Fe wool and showed a similar trend to that of the SF one (see S.M. Section 8 Fig. S14).

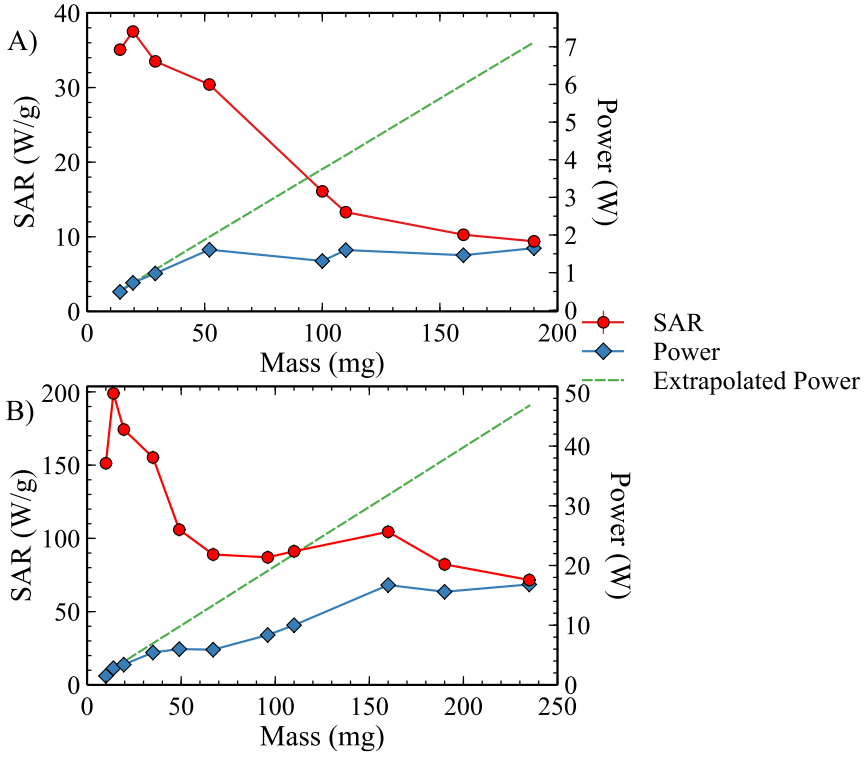

Figure 14: Calorimetric SAR and total power as a function of Fe wool-SF weight under a magnetic field of a) 9.6 mT b) 47.4 mT. Measurements were performed on equipment A at 94 kHz. The dotted line represents the value of the total power under the assumption that the SAR measured for low weight would be maintained for larger weights.

The results are quite complex and deserve a detailed description and discussion. Firstly, and contrarily to what one would expect, the SAR is not weight-independent: it presents maximum values of 38 and 200 W/g under 9.6 and 47.4 mT of field, respectively, when the packed mass is around 15 mg and then starts decreasing for larger values, reaching 10 W/g and 80 W/g for 190 mg of packed Fe wool. In such a case, the total power generated by the sample is an interesting value to be plotted, which has been done in Figure 14. At 9.6 mT, a clear and long plateau is observed: above 50 mg, adding more wool does not increase the total release of heat.

At 47.4 mT, the heating power increases much less than one would expect from a linear relationship between power and mass and then saturates for mass larger than 150 mg.

To show it more clearly, we have added to the plot a dotted line, which represents the total power that would be generated if the SAR value measured for low masses was maintained. When comparing the experimentally generated power values to the expected ones, one clearly sees a large discrepancy: for a 190 mg sample the values are 75% lower under a 9.6 mT field, while for a 240 mg one the values are 64% lower than the expected ones under a 47.4 mT field.

The plotted SAR as a function of mass can be divided into two parts: the first one is a small initial increase of the SAR with mass, the second being a long decrease with mass. We currently have two very different hypotheses to explain these experimental results.

The first one is the influence of magnetic interactions between wires. Indeed, the density of wire increases, which might modify the magnetic susceptibility of the wire assembly. Morales *et al.*[32] have reported that magnetostatic interactions lead to changes in the magnetic behavior of the samples depending on the number of strands. Similarly to our experimental results, they observed an increase in SAR when going from 1 to 5 wires, and then a decrease when going beyond that. This hypothesis might fully explain our data.

Our second hypothesis is very different in nature and would only explain the decrease of SAR with mass. It would be explained by the screening and/or the absorption of the magnetic field applied to the wool strands. One way to understand this effect is to consider that the Fe wool acts like a highly porous bulk material. Thus, increasing the mass of Fe wool in a fixed volume leads to a decrease in the porosity and an increase in the volume density of this supposed bulk material. The magnetic heating of bulk conductive material by eddy currents has already been deeply explored in the literature, and the skin effect is one of the main parameters that governs it[40]. As it is well known, in magnetic and conductive materials, most of the absorbed magnetic field as well as the induced eddy currents are held in the skin depth of the material, which are the most important contributors to the heating. In our hypothesis, for an iron wool mass larger than – let's say – 50 mg, the skin depth of iron wool would be smaller than its radius. The surface layer of Fe wool would therefore absorb most of the magnetic field and act as a screening agent for the wool at the center of the sample. Hence, the Fe wool strand at the center would have a lower heating power than the strands at the surface of the sample.

These results are important for the application of magnetically induced catalysis since they clearly show two crucial points: the first being that increasing the mass of Fe wool (or any micro-scale heating agent for that matter) does not necessarily correspond to an increase in the overall generated heat. Hence, determining the mass above which no gains on heating are obtained is crucial to avoid adding "dead volumes" of heating agents into the reactor. The second point is that the possibility of a non-homogeneous radial heating profile should be envisaged. In fact, if our second hypothesis is correct, the outer part of the reactor would receive more heat than its center, and heat would then have to be transferred towards the center of the reactor by conduction. This type of temperature profile could have implications on the performance of a reactor, in particular when going from lab-scale to pilot-scale applications. In particular, this would diminish the quick reaction time of induction heating compared to

standard one and thus its interest. Our future work will tend to address this issue and discriminate between our two hypotheses.

6. Comparison of Fe wool SAR values with other relevant studies

As was already mentioned, the study of magnetic heating properties of nanoparticles has been extensively investigated in the literature and SAR values of a variety of nanoparticles that are used in magnetic catalysis can be found. The same is not true for micro-scale or larger materials like iron wool or magnetic wires. In this section the SAR values measured on Fe wool will be compared with some other relevant studies of the literature. Only studies that were conducted on iron-based materials as well as under frequencies close to 100 kHz will be considered. Table 2 summarizes the maximum reported SAR value of studied catalysts, their size, and the frequency/field amplitude under which they were measured.

Table 2: Comparison of the magnetic heating power of our samples with other relevant studies of the literature.

Material	Characteristic size (width or diameter)	Frequency/amplitude of the field	SAR (W/g)	SAR/f (J/kg)	Ref.
Fe wool-SF	60 μm	94 kHz/47.4 mT	160	1.7	This study
Fe wool-F	125 μm	94 kHz/47.4 mT	440	4.7	This study
Fe wool-M	225 μm	94 kHz/47.4 mT	700	7.44	This study
FeCo wires	100-300 nm	310 kHz/30 mT	1500	4.83	Alonso *et al.*[33]
$Fe_{71.7}Si_{11}B_{13.4}Nb_3Ni_{0.9}$ microwires	84 μm	310 kHz/70 mT	521	1.68	Talaat *et al.*[34]
Fe(0) nanoparticles	12.5 nm	100 kHz/47 mT	750	7.5	Bordet *et al.*[29]
FeC nanoparticles	15.1 nm	100 kHz/47 mT	3200	32	Bordet *et al.*[29]

In order to better compare the magnetic heating of the different materials under different field frequencies, we added the SAR/*f* values to the table. In the case where only hysteresis losses contribute to heating, SAR/*f* corresponds to the hysteresis area value. We can clearly see that the measured SAR/*f* of Fe wool-M samples is in the range or even higher than one of more expensive materials. For example, Alonso *et al.* reported a value of 4.83 J/kg for their FeCo nanowires, a value 35% lower than the one measured for the M samples, with a higher cost of production. As for Fe(0) nanoparticles, studied by Bordet *et al.*, a maximum SAR/*f* of 7.5 J/kg was measured, which is close to the value of the Fe wool-M sample. Among the various materials reported in Table 2, only the FeC nanoparticles present a considerably higher SAR/f than the Fe wool under a low frequency field. This small comparison shows that Fe wool is a fascinating heating agent for magnetic catalysis applications, with heating power that rival those of more expensive and less stable nano- and micro-scale materials.

IV. Conclusion:

The magnetic heating properties of three types of Fe wool were studied in detail by optical and electronic microscopy, X-Ray diffraction, VSM measurements, heating power and high-frequency hysteresis loop measurements. The effect of various factors linked to the samples

(wire diameter, packing fraction, aspect ratio) and to the external magnetic field (amplitude, frequency, orientation with respect to the sample) were comprehensively studied. The Fe wool strand length and diameter play a major role in the heating power amplitude, with a decrease of the maximum SAR from 530 W/g to 440 W/g when their length goes from 1-1.5 to 0.25-0.5 cm or from 700 W/g to 160 W/g when the diameter is reduced. It was also shown that having the Fe wool strands parallel to the external applied field generates significantly more heat (59% increase under a 47.4 mT field) than when they are perpendicular. High-frequency hysteresis loop measurements were used to estimate the hysteresis losses and eddy current contributions to the sample heating. The results showed that the sample with the largest diameter, Fe wool-M, presents the highest eddy current contribution to heating: 90% contribution under a 50 kHz field frequency. The effect of coating the Fe wool strands was also studied. Adding an insulating coating (SiO_2 or oxidized Ni) has a negative effect on the total heat generation, but no effect on the hysteresis losses of the samples. Lastly, we were able to observe that the packed mass of Fe wool in a given volume plays a major role in the total generated heat as well as on the SAR. Our results showed that adding more Fe wool to the sample leads to a decrease of the measured SAR, with values dropping from 200 W/g to 80 W/g when going from a weight of 15 to 240 mg for the SF sample under a 47.4 mT field. This effect could be due to the absorption and/or screening of the applied field by the surface strands of Fe wool, but also to magnetic interactions. Distinguishing between these two hypotheses will be the work of future studies. Our measurements showed that Fe wool presents large magnetic heating powers that exceed the one of other materials that are more expensive and complex to produce. The results described in this work are useful to better understand the magnetic heating of micro-scale magnetic materials, and to optimize their use in magnetically induced heterogeneous catalysis.

Supplementary materials:

Supplementary results and information that further supports the findings of this study (SAR and hysteresis cycle measurements, used equations, elemental analysis…) can be found in the supplementary materials file.

Acknowledgements:

S.D. thanks ID-Partner and ANRT for CIFRE Grant N° **2021**/0786.

Conflict of interest statement:

The authors have no conflicts of interest.

Data availability:

The data that supports the findings of this study are available within the article and the supplementary materials.

Credit:

Salim Daccache: writing/original draft preparation (lead), writing/review & editing (equal), conceptualization (equal), methodology (equal), investigation (lead), visualization (lead). **Julian Carrey:** writing/original draft preparation (lead), writing/review & editing (equal), conceptualization (equal), supervision (lead), project administration (equal), methodology (equal). **Bruno Chaudret:** writing/review & editing (equal), conceptualization (equal), supervision (equal), project administration (equal). **Sourav Ghosh:** writing/review & editing (equal), conceptualization (equal), resources (equal), visualization (equal). **Frederic Marias:** writing/review & editing (equal), project administration (equal).

References:

[1] H. Ritchie, and M. Roser, "Sector by sector: where do global greenhouse gas emissions come from?," Our World in Data, (2023).
[2]"Clean and efficient heat for industry – Analysis," IEA, (2018).
[3] Md.N.I. Maruf, G. Morales-España, J. Sijm, N. Helistö, and J. Kiviluoma, "Classification, potential role, and modeling of power-to-heat and thermal energy storage in energy systems: A review," Sustainable Energy Technologies and Assessments **53**, 102553 (2022).
[4] R. FARES, "Renewable Energy Intermittency Explained: Challenges, Solutions, and Opportunities - Scientific American Blog Network," (n.d.).
[5] S. Ambec, and C. Crampes, "Real-time electricity pricing to balance green energy intermittency," Energy Economics **94**, 105074 (2021).
[6] A. Fache, F. Marias, and B. Chaudret, "Catalytic reactors for highly exothermic reactions: Steady-state stability enhancement by magnetic induction," CHEMICAL ENGINEERING JOURNAL **390**, (2020).
[7] M. Wei, C.A. McMillan, and S. de la Rue du Can, "Electrification of Industry: Potential, Challenges and Outlook," Curr Sustainable Renewable Energy Rep **6**(4), 140–148 (2019).
[8] V. Rudnev, D. Loveless, and R.L. Cook, *Handbook of Induction Heating*, 2nd ed. (2017).
[9] J. Carrey, B. Mehdaoui, and M. Respaud, "Simple models for dynamic hysteresis loop calculations of magnetic single-domain nanoparticles: Application to magnetic hyperthermia optimization," Journal of Applied Physics **109**(8), 083921 (2011).
[10] V. Connord, B. Mehdaoui, R.P. Tan, J. Carrey, and M. Respaud, "An air-cooled Litz wire coil for measuring the high frequency hysteresis loops of magnetic samples—A useful setup for magnetic hyperthermia applications," Review of Scientific Instruments **85**(9), 093904 (2014).
[11] M. Salaheldeen, A. Nafady, A.M. Abu-Dief, R. Díaz Crespo, M.P. Fernández-García, J.P. Andrés, R. López Antón, J.A. Blanco, and P. Álvarez-Alonso, "Enhancement of Exchange Bias and Perpendicular Magnetic Anisotropy in CoO/Co Multilayer Thin Films by Tuning the Alumina Template Nanohole Size," Nanomaterials **12**(15), 2544 (2022).
[12] A.M. Abu-Dief, M.S.M. Abdelbaky, D. Martínez-Blanco, Z. Amghouz, and S. García-Granda, "Effect of chromium substitution on the structural and magnetic properties of nanocrystalline zinc ferrite," Materials Chemistry and Physics **174**, 164–171 (2016).
[13] H.P. Kok, E.N.K. Cressman, W. Ceelen, C.L. Brace, R. Ivkov, H. Grüll, G. ter Haar, P. Wust, and J. Crezee, "Heating technology for malignant tumors: a review," International Journal of Hyperthermia **37**(1), 711–741 (2020).
[14] C. Sanchez, D. El Hajj Diab, V. Connord, P. Clerc, E. Meunier, B. Pipy, B. Payré, R.P. Tan, M. Gougeon, J. Carrey, V. Gigoux, and D. Fourmy, "Targeting a G-Protein-Coupled Receptor Overexpressed in Endocrine Tumors by Magnetic Nanoparticles To Induce Cell Death," ACS Nano **8**(2), 1350–1363 (2014).

[15] C. Huang, Y. Wang, R. Zhong, Z. Sun, Y. Deng, and L. Duan, “Induction heating enables efficient heterogeneous catalytic reactions over superparamagnetic nanocatalysts,” Chinese Chemical Letters **34**(9), 108101 (2023).
[16] W. Wang, G. Tuci, D. Cuong, Y. Liu, A. Rossin, L. Luconi, J. Nhut, N. Lam, P. Cuong, and G. Giambastiani, “Induction Heating: An Enabling Technology for the Heat Management in Catalytic Processes,” ACS CATALYSIS **9**(9), 7921–7935 (2019).
[17] S. Faure, S.S. Kale, N. Mille, S. Cayez, T. Ourlin, K. Soulantica, J. Carrey, and B. Chaudret, “Improving energy efficiency of magnetic CO2 methanation by modifying coil design, heating agents, and by using eddy currents as the complementary heating source,” Journal of Applied Physics **129**(4), 044901 (2021).
[18] Á. Raya-Barón, S. Ghosh, J. Mazarío, V. Varela-Izquierdo, P.-F. Fazzini, S. Tricard, J. Esvan, and B. Chaudret, “Induction heating: an efficient methodology for the synthesis of functional core–shell nanoparticles,” Mater. Horiz. **10**(11), 4952–4959 (2023).
[19] M. Akdemir, and F. Hansu, “Effect of Induction Heating Aided Dielectric Barrier Discharge on the Elimination of SO2, NOX, and CO Gases,” WATER AIR AND SOIL POLLUTION **231**(1), (2020).
[20] D. Lupu, A. Biris, A. Jianu, C. Bunescu, E. Burkel, E. Indrea, G. Mihailescu, S. Pruneanu, L. Olenic, and I. Misan, “Carbon nanostructures produced by CCVD with induction heating,” CARBON **42**(3), 503–507 (2004).
[21] S.S. Kale, J.M. Asensio, M. Estrader, M. Werner, A. Bordet, D. Yi, J. Marbaix, P.-F. Fazzini, K. Soulantica, and B. Chaudret, “Iron carbide or iron carbide/cobalt nanoparticles for magnetically-induced CO2 hydrogenation over Ni/SiRAlOx catalysts,” Catal. Sci. Technol. **9**(10), 2601–2607 (2019).
[22] W. Wang, C. Duong-Viet, Z. Xu, H. Ba, G. Tuci, G. Giambastiani, Y. Liu, T. Truong-Huu, J.-M. Nhut, and C. Pham-Huu, “CO2 methanation under dynamic operational mode using nickel nanoparticles decorated carbon felt (Ni/OCF) combined with inductive heating,” Catalysis Today **357**, 214–220 (2020).
[23] F. Varsano, M. Bellusci, A. La Barbera, M. Petrecca, M. Albino, and C. Sangregorio, “Dry reforming of methane powered by magnetic induction,” International Journal of Hydrogen Energy **44**(38), 21037–21044 (2019).
[24] P.M. Mortensen, J.S. Engbæk, S.B. Vendelbo, M.F. Hansen, and M. Østberg, “Direct Hysteresis Heating of Catalytically Active Ni–Co Nanoparticles as Steam Reforming Catalyst,” Ind. Eng. Chem. Res. **56**(47), 14006–14013 (2017).
[25] J.M. Asensio, A.B. Miguel, P.-F. Fazzini, P.W.N.M. van Leeuwen, and B. Chaudret, “Hydrodeoxygenation Using Magnetic Induction: High-Temperature Heterogeneous Catalysis in Solution,” Angewandte Chemie International Edition **58**(33), 11306–11310 (2019).
[26] O. Sosa Sabogal, S. Valin, S. Thiery, and S. Salvador, “Design and thermal characterization of an induction-heated reactor for pyrolysis of solid waste,” Chemical Engineering Research and Design **173**, 206–214 (2021).
[27] X. Zuo, H. Ding, J. Zhang, T. Fang, and D. Zhang, “Carbothermal treated iron oxide nanoparticles with improving magnetic heating efficiency for hyperthermia,” Results in Physics **32**, 105095 (2022).
[28] N.A. Usov, R.A. Rytov, and V.A. Bautin, “Properties of assembly of superparamagnetic nanoparticles in viscous liquid,” Sci Rep **11**(1), 6999 (2021).
[29] A. Bordet, L.-M. Lacroix, P.-F. Fazzini, J. Carrey, K. Soulantica, and B. Chaudret, “Magnetically Induced Continuous CO2 Hydrogenation Using Composite Iron Carbide Nanoparticles of Exceptionally High Heating Power,” Angewandte Chemie International Edition **55**(51), 15894–15898 (2016).

[30] J. Marbaix, N. Mille, L.-M. Lacroix, J.M. Asensio, P.-F. Fazzini, K. Soulantica, J. Carrey, and B. Chaudret, "Tuning the Composition of FeCo Nanoparticle Heating Agents for Magnetically Induced Catalysis," ACS Appl. Nano Mater. **3**(4), 3767–3778 (2020).
[31] C. Gómez-Polo, S. Larumbe, J.I. Pérez-Landazábal, and J.M. Pastor, "Analysis of heating effects (magnetic hyperthermia) in FeCrSiBCuNb amorphous and nanocrystalline wires," Journal of Applied Physics **111**(7), 07A314 (2012).
[32] I. Morales, D. Archilla, P. De La Presa, A. Hernando, and P. Marin, "Colossal heating efficiency via eddy currents in amorphous microwires with nearly zero magnetostriction," Sci Rep **10**(1), 602 (2020).
[33] J. Alonso, H. Khurshid, V. Sankar, Z. Nemati, M.H. Phan, E. Garayo, J.A. García, and H. Srikanth, "FeCo nanowires with enhanced heating powers and controllable dimensions for magnetic hyperthermia," Journal of Applied Physics **117**(17), 17D113 (2015).
[34] A. Talaat, J. Alonso, V. Zhukova, E. Garaio, J.A. García, H. Srikanth, M.H. Phan, and A. Zhukov, "Ferromagnetic glass-coated microwires with good heating properties for magnetic hyperthermia," Sci Rep **6**(1), 39300 (2016).
[35] S. Ghosh, T. Ourlin, J. Mazarío, S. Cayez, S. Daccache, J. Carrey, and B. Chaudret, "Fe@SiO2@Ni: An Iron-Based Composite Material for Magnetically Induced Hydrogenation Reactions in Gas and Solution Phases," Chem. Mater. **35**(18), 7542–7553 (2023).
[36] S. Ghosh, T. Ourlin, P.-F. Fazzini, L.-M. Lacroix, S. Tricard, J. Esvan, S. Cayez, and B. Chaudret, "Magnetically Induced CO2 Methanation In Continuous Flow Over Supported Nickel Catalysts with Improved Energy Efficiency," ChemSusChem **16**(1), e202201724 (2023).
[37] S. Ghosh, S. Gupta, M. Gregoire, T. Ourlin, P.-F. Fazzini, E. Abi-Aad, C. Poupin, and B. Chaudret, "Catalytic Sabatier Process under Thermally and Magnetically Induced Heating: A Comparative Case Study for Titania-Supported Nickel Catalyst," Nanomaterials **13**(9), 1474 (2023).
[38] F. Fiorillo, "Chapter 2 - Soft Magnetic Materials," in *Characterization and Measurement of Magnetic Materials*, edited by F. Fiorillo, (Academic Press, San Diego, 2004), pp. 25–88.
[39] L.-M. Lacroix, J. Carrey, and M. Respaud, "A frequency-adjustable electromagnet for hyperthermia measurements on magnetic nanoparticles," Review of Scientific Instruments **79**(9), 093909 (2008).
[40] J. Delacroix, P. Piluso, N. Chikhi, and P. Fouquart, "Induction heating of cylindrical loads of arbitrary skin-depth by 'current-sheet' inductors," Electr Eng **100**(2), 811–822 (2018).